Simulating Quantum Many-Body Dynamics on a Current Digital Quantum Computer

Alessandro Palermo: 03770455
Chiara Ballotta: 03774192
Chenshuo Ma: 03766391

Advanced Lab Course - Master of Physics
Winter Semester 2023/2024

Faculty of Physics
Technical University Munich

Munich, January 15, 2024

Contents

Introduction

This FOPRA consist in a series of exercises to simulate operations on a current quantum computer, using the library Qiskit in Python (`https://www.ibm.com/quantum/qiskit`). The project starts from some basics circuits of Quantum Information, such as Bell states preparation, quantum teleportation and Rabi oscillations. Gradually the tasks becomes more advanced and focused on the difference between a simulation, in which we have direct access to the wavefunctions, and a real quantum computer, where the only way to evaluate the relevant observables is measuring the qubits several times, in a noisy environment. At the end of Day 1, we exploit a Variation Quantum Eigensolver algorithm to find the ground state of a specific Hamiltonian. Day 2 is dedicated to simulate a many-body dynamic (transversal field Ising 1D chain): varying some parameters (number of qubits, strength of the interaction) a dynamical quantum phase transition is observed and finally the increase of entropy of the system is evaluated.

1 First day

1.1 Error mitigation

Exercise 1

The readout matrix unfolding is a simple, yet effective protocol for error mitigation, it consists of a calibration and unfolding part. During calibration, an initial state b is prepared from the computational basis, and then every qubit is measured, obtaining a string a, which accounts for eventual errors. After m iterations, the results of the calibration can be written in a matrix form P_{ab} = Pr(Measured bitstring a | Prepared bitstring b). The unfolding step consists of using P_{ab} to mitigate errors after measurements in a real quantum circuit: calling v' the vector of measured probabilities and v the error-free ones, they are related by: $v'_a = \sum_b P_{ab} v_b$

If the elements of the measured v' sums to unity: $\sum_a v'_a = 1$, it can be shown that the inverted v_a preserve the sum: $\sum_a v_a = 1$, this is due to conservation of probability, forcing P to be doubly stochastic. In particular, for a chosen b,

$$\sum_a P_{ab} = 1$$

since whatever state b we prepare, the total probability of all the measurement outcomes must sum up to one. Thus we see that

$$\begin{aligned} \sum_a v'_a &= \sum_{ab} P_{ab} v_b \\ &= \sum_b v_b \sum_a P_{ab} \\ &= \sum_b v_b \end{aligned} \tag{1}$$

and thus $\sum_a v'_a = 1$ implies $\sum_a v_a = 1$.

1.2 Quantum teleportation

Exercise 2

Up to a global phase the four Bell states are related to each other by single-qubit Pauli gates: $\mathbb{1} \otimes \sigma_\alpha$, where $\alpha = x, y, z$. Therefore once we find the circuit to create one of them, the other differ just by a single qubit gate, as reported in Figure 1. Note that a 2-qubit gate, such as a CNOT, is necessary to create entanglement between the two qubits.

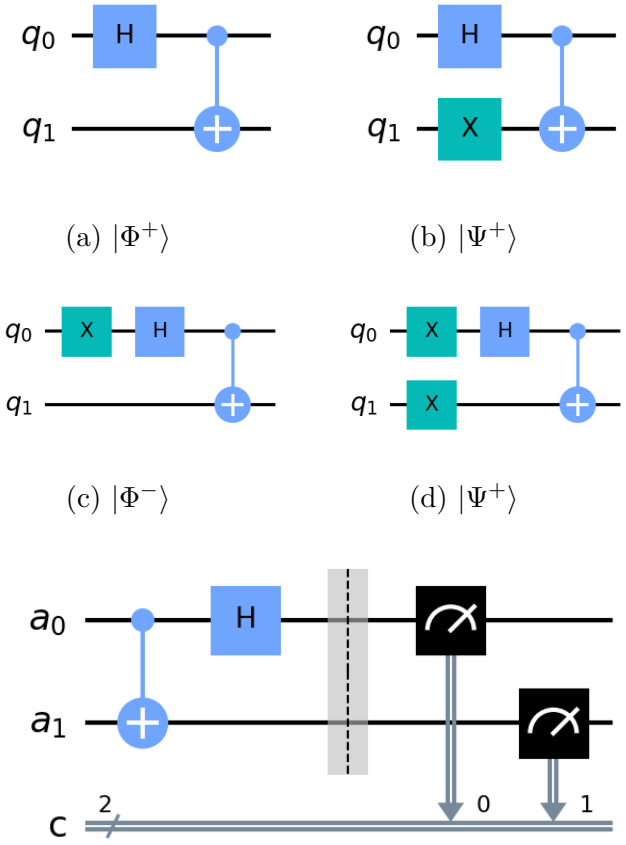

(a) $|\Phi^+\rangle$ (b) $|\Psi^+\rangle$

(c) $|\Phi^-\rangle$ (d) $|\Psi^+\rangle$

(e) Bell measurement

Figure 1: Bell states preparation (a) to (d) and Bell state measurement (e).

state	qubit a_0	qubit a_1	unitary to decode state
$\|\Phi^+\rangle$	0	0	$\mathbb{1}$
$\|\Phi^-\rangle$	1	0	σ_z
$\|\Psi^+\rangle$	0	1	σ_x
$\|\Psi^-\rangle$	1	1	σ_y

Table 1: Bell state measurement and conditional operation for quantum teleportation.

To measure the state of Alice's qubits, we perform a so-called "Bell measurement", with a circuit diagram as the one reported in Figure 1e. Outcomes and results are related in Table 1, together with the unitary Bob needs to apply to reconstruct the original state.

To see why the four Bell states give rise to the four bitstrings in Table 1, we notice that the Bell measurement simply reverses the Hadamard - CNOT entangling gate sequence in Figure 1, and we are left with the four possible combinations of the Pauli-X gate.

To justify our correction unitaries, we use the following identity:

$$\left({}_{a_0a_1}\langle\Phi_+|\mathbb{1}\otimes\sigma_\alpha\right)|\Phi_+\rangle_{a_1b}\,|\psi\rangle_{a_0} \propto \sigma_\alpha\,|\psi\rangle_b \tag{2}$$

which is derived by applying the following "transposition" trick: $\mathbb{1}\otimes\sigma_\alpha\,|\Phi_+\rangle = \sigma_\alpha^T\otimes\mathbb{1}\,|\Phi_+\rangle$.

Exercise 3

The full teleportation circuit is presented in Figure 2. A random state $|\Psi\rangle$ is prepared in qubit a_0, and a maximally entangled state is shared between qubit a_1 and b. After that, a Bell measurement is performed on Alice's qubits, and one of the four Paulis is applied to recover the state $|\psi\rangle$. The Bloch spheres in Figure 3 compare the original state in a_0 with the final state of the qubits at the end of the protocol: qubit a_0 and a_1 are collapsed after the measurement, either to $|0\rangle$ or $|1\rangle$, and $|\psi\rangle$ is teleported to qubit b.

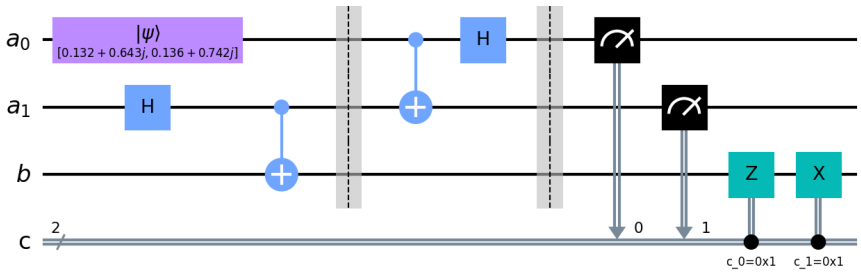

Figure 2: Circuit for quantum teleportation protocol.

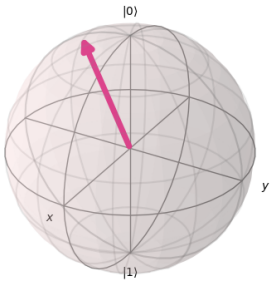

(a)

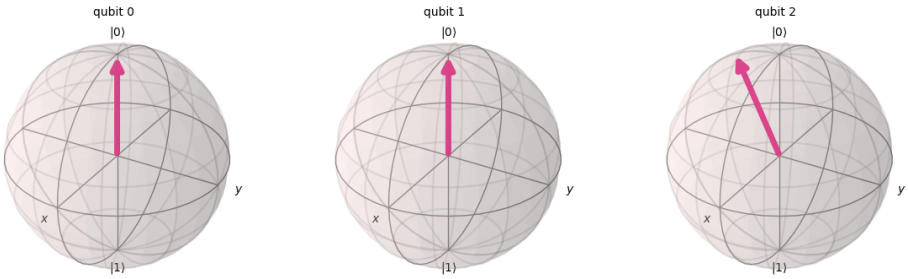

(b)

Figure 3: Original state to be teleported (a) and final states of the qubits (b). Still in (b), qubits 0, 1 and 2 coincide respectively to qubits a_0, a_1 and b from the teleportation circuit in Figure 2 and in the main text.

1.3 Rabi Oscillation

Exercise 4

Let's consider a qubit driven by the Hamiltonian: $\hat{H} = -\frac{\omega_0}{2}\hat{\sigma}_z + \omega_1 \cos(\omega t)\hat{\sigma}_x$, where ω_0 is the qubit frequency, understood as the energy difference between the two levels, and ω, ω_1 represent the drive frequency and drive strength respectively. The generalized Rabi frequency includes the detuning $\Delta = \omega - \omega_0$, and is found by $\Omega = \sqrt{\omega_1^2 + \Delta^2}$.

For a general state $|\Psi\rangle = \alpha|0\rangle + \beta|1\rangle$, the time evolution in rotating wave approximation is given by:

$$e^{-i\omega t/2}\alpha(t) = \cos\left(\frac{\Omega t}{2}\right) - \frac{i\Delta}{\Omega}\sin\left(\frac{\Omega t}{2}\right) \tag{3}$$

$$e^{i\omega t/2}\beta(t) = -\frac{i\omega_1}{\Omega}\sin\left(\frac{\Omega t}{2}\right) \tag{4}$$

The population of ground and excited state with time is given respectively by the square modulus of α and β:

$$P_1 = \left(\frac{\omega_1}{\Omega}\right)^2 \sin^2\left(\frac{\Omega t}{2}\right) \tag{5}$$

$$P_0 = 1 - P_1 \tag{6}$$

Exercise 5

Using a time dependent Trotterization it is possible to efficiently simulate the time evolution of the system. The time evolution operator U is approximated by alternating the time evolutions generated by the two non-commuting terms in the Hamiltonian for small time steps.

(a) The analytical result is compared to the simulation in Figure 4a for the following parameters: $\omega_1 = 2$, $\omega_0 = 25$, $\omega = 25.5$ for $t \in [0, 4]$, and time step $\delta t = 0.05$.

(b) By sweeping the drive frequency $\omega \in [10, 40]$, we probe the resonance of this two level system by applying the pulse for $t = \pi/\omega_1$. On resonance, this simply executes a π pulse, and as we move out from the resonant frequency, we begin to see the characteristic sinc-like response in Fig. 4b

(c) Moreover using the parameters $\omega = \omega_0 = \omega_1 = 2$, the analytic solution clearly differs from the trotterized result in Fig 4c. The Trotterization is doing just fine since we haven't changed the timestep; instead, the rotating wave approximation fails at this parameter regime since with ω being much smaller, the terms proportional to $e^{\pm 2i\omega t}$ in the interaction picture Hamitonian (frame of the magnetic field) are no longer "rapidly oscillating". This high frequency assumption was what allowed the previous two cases to work, since at the same timescales, higher frequency contributions tend to cancel out.

In fact, observing Fig. 4b, we notice that RWA results don't fit with the Trotterized results very well in the low frequency regime! This again reflects the exact same mechanism at work.

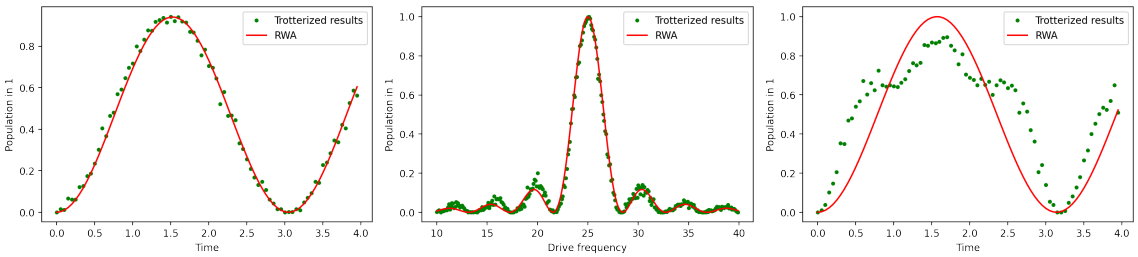

(a) Time evolution (b) Detuning (c) Time evolution 2

Figure 4: Simulated population signals for a) time evolution, b) resonance sweeping, and c) low qubit/drive frequency

Exercise 6

Next step consists in introducing noise in the simulation. Interaction with the environment is one of the main cause of errors and can be modeled as a generalized amplitude damping quantum channel, acting on the density matrix representing our qubit as follows:

$$\Lambda(\rho) = \sum_{i=0}^{3} E_i \rho E_i^{\dagger} \tag{7}$$

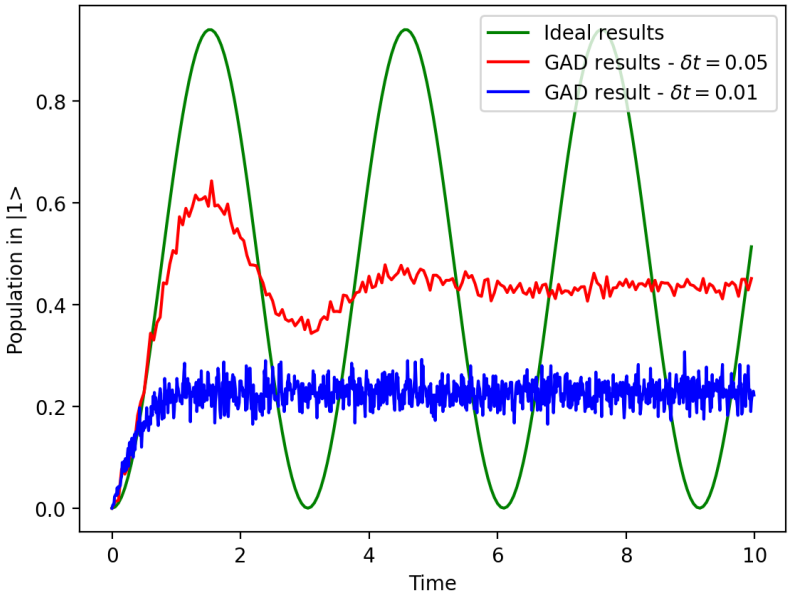

Figure 5: Simulation of Rabi oscillation with noise at different time steps.

with

$$E_0 = \sqrt{1-p}\begin{bmatrix} 1 & 0 \\ 0 & \sqrt{1-\gamma} \end{bmatrix}, \quad E_2 = \sqrt{p}\begin{bmatrix} \sqrt{1-\gamma} & 0 \\ 0 & 1 \end{bmatrix}$$
$$E_1 = \sqrt{1-p}\begin{bmatrix} 0 & \sqrt{\gamma} \\ 0 & 0 \end{bmatrix}, \qquad E_3 = \sqrt{p}\begin{bmatrix} 0 & 0 \\ \sqrt{\gamma} & 0 \end{bmatrix} \tag{8}$$

where $p \in [0, 1]$ quantifies the probability for thermal excitation and $\gamma \in [0, 1]$ is the probability of losing energy to the environment, e.g. via spontaneous emission. For our simulation we set $p = 0.1$, $\gamma = 0.02$ and use the same parameters as Exercise 5(a). The results are shown in Figure 5 for different time steps: 0.05 s (red) and 0.01 s (blue), against the ideal result (green). The effect of noise is to damp the oscillation over time, reaching a steady state in approximately 6 seconds and 1.5 seconds, respectively, given by the equilibrium of driving field and spontaneous emission. Since noisy gates are applied at every time step of the Trotterization, for smaller time steps the effect of noise is increased, and oscillation amplitude decreases faster.

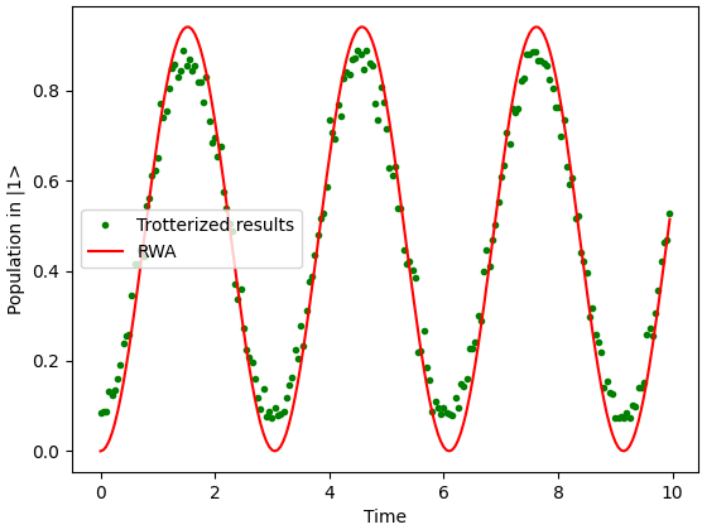

Figure 6: Simulation of Rabi oscillation with noise from a real quantum system

Exercise 7

It is also possible to include in the simulation a realistic noise models from a real quantum device, in this case IBM Vigo, a superconducting, 5-qubit system. Since we are driving just one qubit we are not interested in the topology of the system, apart from eventual crosstalks between qubits which induce another eventual source of errors. Results of the simulation with this noise model are reported in Figure 6. In this case, damping of the oscillations is much less pronounced than in the case of general amplitude damping channel, depicting a situation with less noise and more reliable qubits.

1.4 Single-qubit Tomography

Exercise 8

The operation to reconstruct the state of a qubit in a pure or in a mixed state is called quantum state tomography and consists of measuring the density matrix of the qubit ρ in the orthogonal basis (by the Hilbert-Schmidt inner product) given by the Pauli matrices. In fact, we can write $\rho = 1/2\,(\mathbb{1} + \sum_i c_i\sigma_i)$, and the coefficients are given by $c_i = \mathrm{Tr}(\rho\sigma_i)$. However a single measurement only gives output 0 or 1 since the state collapses: to obtain a precise result, the measurement on each element of the basis must be repeated several times and the results averaged.

Measurement in a quantum computer probe the eigenstates of σ_z, to be able to measure $\langle\sigma_x\rangle$ and $\langle\sigma_y\rangle$ we need to perform a base transformation given by the following:

$$X = HZH, \qquad Y = SHZHS^\dagger = SXS^\dagger \tag{9}$$

We can explicitly verify the previous relation using the matrix representation of the operators

$$X = \begin{pmatrix} 0 & 1 \\ 1 & 0 \end{pmatrix} = \frac{1}{\sqrt{2}}\begin{pmatrix} 1 & 1 \\ 1 & -1 \end{pmatrix}\begin{pmatrix} 1 & 0 \\ 0 & -1 \end{pmatrix}\frac{1}{\sqrt{2}}\begin{pmatrix} 1 & 1 \\ 1 & -1 \end{pmatrix} \tag{10}$$

$$Y = \begin{pmatrix} 0 & -i \\ i & 0 \end{pmatrix} = \begin{pmatrix} 1 & 0 \\ 0 & i \end{pmatrix}\begin{pmatrix} 0 & 1 \\ 1 & 0 \end{pmatrix}\begin{pmatrix} 1 & 0 \\ 0 & -i \end{pmatrix} \tag{11}$$

Thus we measure $\langle\sigma_z\rangle$ by just counting $p_0 - p_1$ in the measurement statistics, and $\langle\sigma_x\rangle$, $\langle\sigma_y\rangle$ by applying H and $HS^\dagger$ before measuring (see code).

Exercise 9

We used the single-qubit tomography method from the previous exercise to reconstruct the single-qubit density matrix for the pure state $\frac{1}{\sqrt{2}}\left(|0\rangle + e^{i\pi/4}|1\rangle\right) = TH|0\rangle$

After obtaining the Bloch vector $\vec{c}$ from finite sampling, we renormalize it to compensate for statistical errors, justified by the fact that we did in fact prepare a pure state. Then the density matrix is re-assembled as $\rho = 1/2\,(\mathbb{1} + \sum_i c_i\sigma_i)$.

To extract the qubit statevector, we take the renormalized Bloch vector components and infer the pure state $\cos(\theta/2)\,|0\rangle + e^{i\phi}\sin(\theta/2)\,|1\rangle$ using $\theta = \arccos(c_z)$ and $\phi = \arctan(c_y/c_x)$.

Benchmarking with qiskit's state tomography function "StateTomography()", we computed the trace distance of our density matrix ρ and qiskit's version ρ_Q, and found that $\mathrm{Tr}\left(\sqrt{(\rho-\rho_Q)^2}\right)^2 < 0.001$, proving the robustness of our implementation.

Exercise 10

We used Quantum State Tomography to reconstruct the evolution of a qubit during detuned Rabi Oscillation (same parameters as in Exercise 5(a) for $t \in [0, 2]$), the result are plotted in Figure 7. The data points follow the general behaviour of the evolution, with small deviation explained by the finite amount of averaging in the state tomography.

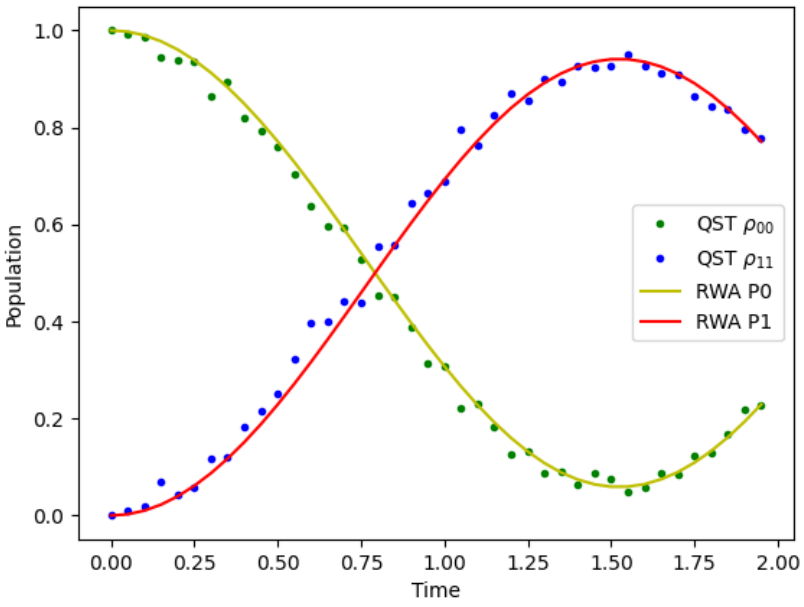

Figure 7: State tomography of Rabi Oscillations as in Exercise 5(a).

1.5 Variational Quantum Eigensolver

Exercise 11

One common procedure to approximate the ground state of a local Hamiltonian $\hat{H}$ is the variational method: the energy of a parameterized ansatz $|\psi(\theta)\rangle$ is evaluated and minimized over the parameter space of θ. However the estimation of the energy $\langle\psi(\theta)|\hat{H}|\psi(\theta)\rangle$ is exponentially hard for N qubits on a classical computer, therefore in a Variational Quantum Eigensolver (VQE) algorithm this step is left to a quantum hardware.

Let's consider the following two qubit Hamiltonian and trial state:

$$\hat{H} = -\sigma_x^1\sigma_z^2 - \sigma_z^1\sigma_x^2 \tag{12}$$

$$|\Psi(\theta)\rangle = e^{ia(\sigma_z^1+\sigma_z^2)}e^{ib(\sigma_x^1\sigma_z^2+\sigma_z^1\sigma_x^2)}\,|00\rangle \tag{13}$$

where $a, b \in \mathbb{R}$. The parametrized quantum circuit (PQC) that construct this ansatz is depicted is Figure 8 for a,b = 1.

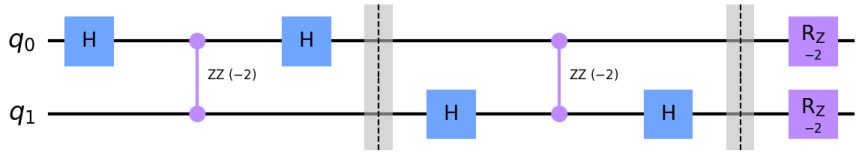

Figure 8: Quantum circuit to construct the Ansatz state of Eq. 13

To see the equivalence of our PQC and Equation 13, we notice that the cluster Hamiltonian consists of two commuting terms, and thus its time evolution factors as

$$e^{ib(\sigma_x^1\sigma_z^2+\sigma_z^1\sigma_x^2)} = e^{ib\sigma_z^1\sigma_x^2}e^{ib\sigma_x^1\sigma_z^2}$$

Now we again use the identity that conjugation by the Hadamard transforms σ_x to σ_z and vice versa:

$$e^{ib\sigma_z^1\sigma_x^2} = H^2e^{ib\sigma_z^1\sigma_z^2}H^2$$

which can be explicitly proven by something like a power series expansion. The first two sections of the circuit (according to the barriers) therefore implement $e^{ib(\sigma_x^1\sigma_z^2+\sigma_z^1\sigma_x^2)}$, and the last section implements the local unitaries.

Exercise 12

Varying the values of a and b in the range $a, b \in [0, \pi]$ and calculating the expectation value of the Hamiltonian for each combination, we obtain the colormap in Figure 9. The minimum values are reached for $(a_1, b_1) = (\pi/4, \pi/4)$ and $(a_2, b_2) = (0.7\pi, 0.7\pi)$, for which the approximated ground state energy is

$$\langle\psi(a_1, b_1)|\hat{H}|\psi(a_1, b_1)\rangle = \langle\psi(a_2, b_2)|\hat{H}|\psi(a_2, b_2)\rangle \approx -1.99$$

The approximated state reaching the minimum is

$$\begin{aligned}|\psi(a_1, b_1)\rangle \cong (-3.79 \times 10^{-2} + 0.457i)\,|00\rangle + (1.11 \times 10^{-16} + 0.498i)\,|01\rangle \\ +(8.33 \times 10^{-17} + 0.498i)\,|10\rangle + (-4.47 \times 10^{-2} - 0.539i)\,|11\rangle\end{aligned}$$

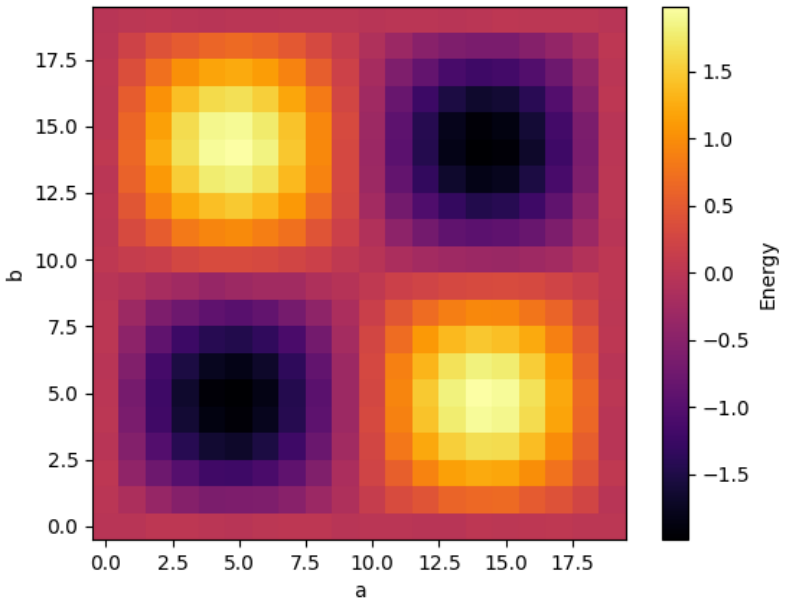

Figure 9: Expectation value of the Hamiltonian $\langle\psi(a, b)|\,\hat{H}\,|\psi(a, b)\rangle$ over a and b varying between 0 and π. The axes are in unit of $\pi/20$.

We compare this with the exact ground state of this Hamiltonian, obtained by direct observation:

$$\hat{H} = -H^1\left(\sigma_x^1\sigma_x^2 + \sigma_z^1\sigma_z^2\right)H^1$$

and since it is frustration free, we have the ground state as $H \otimes \mathbb{1} \left|\Phi_+\right\rangle$ since $\left|\Phi_+\right\rangle$ is the unique state stabilized by both terms after the local Hadamard. Due to the coarse nature of the direct search, this can not be exactly expressed by the parameterized state in Equation 13.

Exercise 13

The exact ground state of the Hamiltonian can be also computed via diagonalization. The 2 qubit Hamiltonian $\hat{H}$ can be written in matrix representation in a 4-dimensional space as:

$$\hat{H} = -\sigma_x^1\sigma_z^2 - \sigma_z^1\sigma_x^2 = \begin{pmatrix} 0 & -1 & -1 & 0 \\ -1 & 0 & 0 & 1 \\ -1 & 0 & 0 & 1 \\ 0 & 1 & 1 & 0 \end{pmatrix} \tag{14}$$

where we have assumed $|00\rangle = (1,0,0,0)^T, |01\rangle = (0,1,0,0)^T, |10\rangle = (0,0,1,0)^T, |11\rangle = (0,0,0,1)^T$. The matrix can be exactly diagonalized with eigenvalues 0 (doubly degenerate) and ± 2, where the eigenvector corresponding to the minimum eigenvalue is $\vec{v} = \frac{1}{2}(1,1,1,-1)$, which corresponding to $|\Psi_{\text{exact}}\rangle = \frac{1}{\sqrt{2}}(|0+\rangle + |1-\rangle) = \frac{1}{2}(|00\rangle + |01\rangle + |10\rangle - |11\rangle)$, where $|\pm\rangle = \frac{1}{\sqrt{2}}(|0\rangle \pm |1\rangle)$. Our approximate result looks similar to $|\Psi_{\text{exact}}\rangle$ once we neglect the small real parts (in every term smaller than 5×10^{-2}) and we cross out a global phase. In fact after this simplifications and re-normalization the approximate wavefunction becomes $|\psi(a_1, b_1)\rangle \sim 0.459\,|00\rangle + 0.500\,|01\rangle + 0.500\,|10\rangle - 0.541\,|11\rangle$

Exercise 14

The simulation of Exercise 12 can be repeated in a noisy environment. We used the same error model of Exercise 6 with $p = 0.2$ (thermal excitation) and $\gamma = 0.1$ (spontaneous emission). The new simulation is shown in Figure 10. The energy landscape is qualitatively identical to the previous of Figure 9, with maxima and minima in the same positions, thus same wavefunction minimizing the energy. However the amplitude of the eigenenergies is drastically reduced, as we note from the colourbar,

with minimum energy equal to -1.31. This reflects the robustness of PQCs against un-correlated noise.

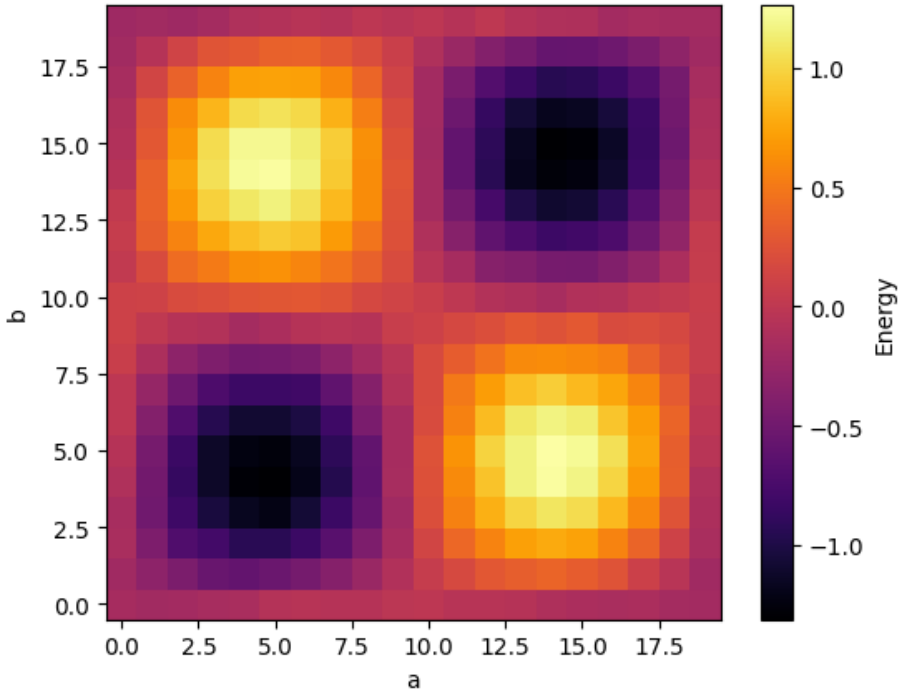

Figure 10: Expectation value of the Hamiltonian $\langle\psi(a,b)|\,\hat{H}\,|\psi(a,b)\rangle$, in a noisy simulation over a and b varying between 0 and π. The axes have unit of $\pi/20$.

2 Second day

2.1 Dynamical Quantum Phase Transitions

Exercise 1

Given the Loschmidt amplitude $\mathcal{G}(t) = \langle\Psi_0|\Psi_0(t)\rangle = \langle\Psi_0|e^{-i\hat{H}t}|\Psi_0\rangle$ and the Loschmidt echo $\mathcal{L}(t) = |\mathcal{G}(t)|^2$, in the thermodynamic limit these quantities scale as $\mathcal{G}(t) = e^{-Ng(t)}$ and $\mathcal{L}(t) = e^{-N\lambda(t)}$. Using these we have

$$\begin{aligned} e^{-N\lambda(t)} &= |e^{-Ng(t)}|^2 \\ &= e^{-Ng(t)}e^{-Ng^*(t)} \\ &= e^{-N(g(t)+g^*(t))} \\ &= e^{-2NRe(g(t))} \end{aligned}$$

and therefore $\lambda(t) = 2Re(g(t))$

Exercise 2

If the initial Hamiltonian $\hat{H}_0$ has more than one ground state, as in the case of spontaneous symmetry breaking, the Loschmidt echo becomes:

$$\mathcal{L}(t) = \sum_{i=1}^{N_{gs}} |\langle\Psi_i|\Psi_0(t)\rangle|^2$$

where $|\Psi_i\rangle, i = 1, ..., N_{gs}$ labels the N_{gs} states in the ground state manifold of $\hat{H}_0$. We can then define the individual Loschmidt rates as

$$|\langle\Psi_i|\Psi_0(t)\rangle|^2 = e^{-N\lambda_i(t)}$$

The usual Loschmidt rate is written as

$$\begin{aligned}\lambda(t) &= -\lim_{N\to\infty}\frac{1}{N}\log\mathcal{L}(t)\\ &= -\lim_{N\to\infty}\frac{1}{N}\log\left(\sum_{i=1}^{N_{gs}}|\langle\Psi_i|\Psi_0(t)\rangle|^2\right)\\ &= -\lim_{N\to\infty}\frac{1}{N}\log\left(\sum_{i=1}^{N_{gs}}e^{-N\lambda_i(t)}\right)\end{aligned}$$

For $N\to\infty$, all terms in the sum except for the minimum λ_i are exponentially suppressed:

$$\begin{aligned}\lim_{N\to\infty}\lambda(t) &= -\frac{1}{N}\log\Big(\max_i[e^{-N\lambda_i(t)}]\Big)\\ &= -\frac{1}{N}\log\big(e^{-N\min_i[\lambda_i(t)]}\big)\\ &= \min_i[\lambda_i(t)]\end{aligned}$$

2.2 The transverse field Ising model

Exercise 3

Let's consider a 1-dimensional Ising chain of N qubits with transverse field . The Hamiltonian of the system is given by:

$$\hat{H} = -\frac{1}{2}\sum_{\langle i,j\rangle}Z_iZ_j - \frac{g}{2}\sum_i X_i \tag{15}$$

where $\langle i,j\rangle$ denotes nearest neighbours sites, the ZZ Ising interaction is set to unity whereas the transverse field strength is parametrized by g. It can be shown that the parity operator:

$$\hat{P} = \prod_i X_i$$

commutes with the Hamiltonian. In particular it can be seen immediately that the transverse part of the Hamiltonian commutes with $\hat{P}$, since they are both composed just by X_i terms. For the Z_iZ_j terms we can write:

$$[\hat{H},\hat{P}] = \left[-\frac{1}{2}\sum_{\langle i,j\rangle} Z_iZ_j,\hat{P}\right] + \left[-\frac{g}{2}\sum_i X_i,\hat{P}\right] = \left[-\frac{1}{2}\sum_{\langle i,j\rangle} Z_iZ_j,\hat{P}\right] + 0 =$$
$$= \left(-\frac{1}{2}\sum_{\langle i,j\rangle} Z_iZ_j\right)\prod_{i'} X_{i'} - \prod_{i'} X_{i'}\left(-\frac{1}{2}\sum_{\langle i,j\rangle} Z_iZ_j\right) =$$
$$= -\frac{1}{2}\sum_{\langle i,j\rangle}\left(Y_iY_j\prod_{i'\neq i,j} X_{i'}\right) + \frac{1}{2}\sum_{\langle i,j\rangle}\left(\prod_{i'\neq i,j} X_{i'}\right)(-Y_i)(-Y_j) = 0$$

The spectrum of $\hat{P}$ is just $\{\pm 1\}$ since it is an Hermitian element of the Pauli group, and its eigenstates are given by the 2^N combinations of $|\pm x\rangle$ states on each site.

For $g \to 0$ the ground state of $\hat{H}$ is doubly degenerate and is given by all the qubits in $|00...0\rangle$ or $|11...1\rangle$, with magnetization respectively at $\langle m_z\rangle = 1$ and $\langle m_z\rangle = -1$.

For $g \to \infty$ the ground state is given by all qubits aligned parallel to the field: $|+\rangle^{\otimes N}$, and the magnetization is $\langle m_z\rangle = 0$.

Exercise 4

Let's use the Kramers-Wannier duality transformation to rewrite the Hamiltonian in terms of the new Ising variables:

$$\tilde{Z}_n = \prod_{i\leq n} X_i \qquad \tilde{X}_n = Z_nZ_{n+1}$$

Firstly, we show that $\{\tilde{Z}_n,\tilde{X}_n\} = 0$:

$$\{\tilde{Z}_n,\tilde{X}_n\} = \tilde{Z}_n\tilde{X}_n + \tilde{X}_n\tilde{Z}_n = \left(\prod_{i\leq n} X_i\right) Z_nZ_{n+1} + Z_nZ_{n+1}\left(\prod_{i\leq n} X_i\right) =$$
$$= \left(\prod_{i<n} X_i\right) X_nZ_nZ_{n+1} + Z_nZ_{n+1}\left(\prod_{i<n} X_i\right) X_n = \left(\prod_{i<n} X_i\right) Z_{n+1}\{X_n,Z_n\} = 0$$

So the new operators satisfy the same anticommutation relation of the original varables: $\{X_i,Z_i\} = 0$. In an infinite 1D chain the term $\hat{H} = -\frac{1}{2}\sum_{\langle i,j\rangle} Z_iZ_j$ immediately

becomes $-\frac{1}{2}\sum_n \tilde{X}_n$, since the index j in the original sum just assumes values $i+1$. Moreover, since $X_i X_i = \mathbb{1}$, each X_i can be written as $X_i = \left(\prod_{j\leq i-1} X_j\right)\left(\prod_{j\leq i} X_j\right) = \tilde{Z}_{i-1}\tilde{Z}_i$.

So the whole Hamiltonian becomes

$$\hat{H} = -\frac{1}{2}\sum_n \tilde{X}_n - \frac{g}{2}\sum_n \tilde{Z}_n\tilde{Z}_{n+1} \tag{16}$$

Compared to the original Hamiltonian (Equation 15), the transformed one is identical, up to an overall scaling and the transverse field strength $g' = 1/g$:

$$\hat{H} \propto -\frac{1}{2}\sum_n \tilde{Z}_n\tilde{Z}_{n+1} - \frac{1}{2g}\sum_n \tilde{X}_n$$

Thus, if the TFI model has a critical point at g, the dual model has the exact same critical point at $1/g$. We further assume that there is only one such critical point transitioning into the ferromagnetic phase, which seems reasonable since the system's reaction to an increasing transverse field should intuitively be monotonous. The location of this point can therefore be found by solving $g = 1/g$, or $g = 1$.

In particular for $g = 1$, the two expression looks formally the same. Analyzing the behaviour of the ground state at the limits $g \to 0$ and $g \to \infty$ we find all the spins aligned respectively to the $\tilde{X}$ and to the $\tilde{Z}$ axis (with double degeneracy), apparently in contradictions to the previous case, before the Kramers-Wannier duality. This shows that for $g = 1$, when the Hamiltonians shows the same structure in the duality, their behaviour must coincide and $g_c = 1$ is the critical field.

Exercise 5

For $T = 0$ and $g < 1$ the system shows ferromagnetic order in the ground state. However this configuration does not survive at finite temperature. To show this, let us introduce two domains in our spin chain with opposite spin orientation up or down. From Equation 15, the energy difference from the ground state associated with the domain wall is $\Delta E = 1/2$. The creation of a domain wall introduces also a difference in the entropy of the system; in particular, for a chain with N sites, we can choose

the position of the domain wall in N different ways, so $\Delta S = k_b \log(N)$. Therefore the free energy difference of a state of two domains compared to the single domain ferromagnetic ordered state is $\Delta F = \Delta E - T\Delta S = \Delta E - k_b T \log(N)$. Since ΔE does not depend on N, the entropy term always prevails for a sufficient long chain at any $T > 0$, and long range ferromagnetic order is not favourable.

Alternatively, we can compute the free energy of a state with s domain walls:

$$\begin{aligned} F &= s\Delta E - TS \\ &= s\Delta E - k_B T \log \binom{N}{s} \\ &\approx s\left(\Delta E - k_B T(\log(N) - \log(s))\right) \end{aligned}$$

where in the last step we approximated the binomial coefficient with $\frac{N^s}{s!}$ assuming $s \ll N$, and then used Sterling's formula approximating $\log(s!) \approx s \log s$. Thus at low temperatures, we expect $s \sim N \exp(-\Delta E / k_B T)$. Notice that this quantity is directly proportional to the system size, and the only other relevant variable is temperature.

2.3 DQPT in the TFI using Qiskit

Exercise 6

We want now to implement the time evolution of the Tranverse Field Ising (TFI) Hamiltonian (Equation 15) in Qiskit, performing a Trotter decomposition:

$$U(t) = \left(e^{-i\hat{H}dt}\right)^{t/dt} \approx \left(e^{\hat{A}+\hat{B}}\right)^{t/dt}$$

with $\hat{A} = i\,dt\,\frac{g}{2}\sum_i X_i$, $\hat{B} = i\,dt\,\frac{1}{2}\sum_{<i,j>} Z_i Z_j$ and using the RX and RZZ gates.

Figures 11 and 12 show two circuits for $N = 4$ qubit implementing the evolution of the system by a small time step dt; using respectively a first order Trotterization $e^{\hat{A}+\hat{B}} = e^{\hat{A}} e^{\hat{B}}$ and the second order trotterization $e^{\hat{A}+\hat{B}} = e^{\hat{A}/2} e^{\hat{B}} e^{\hat{A}/2}$ for the following parameters: $g = 2$, $dt = 0.05$.

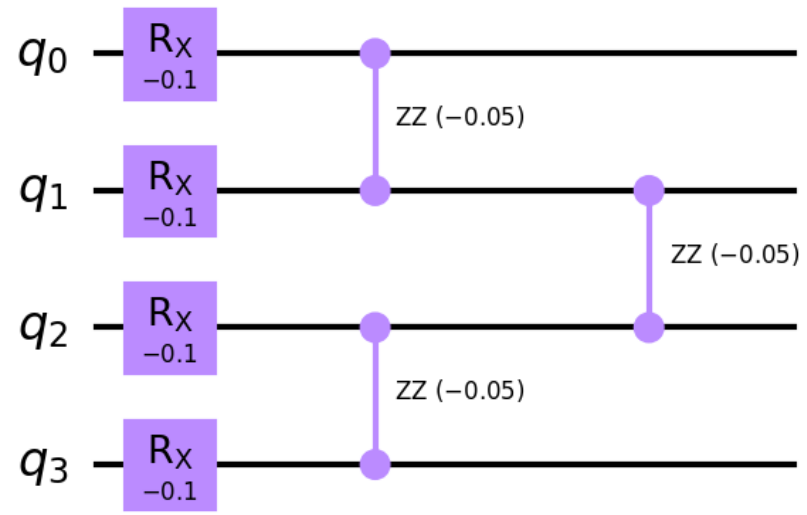

Figure 11: First order trotterization step, which evolve the state for a time step dt.

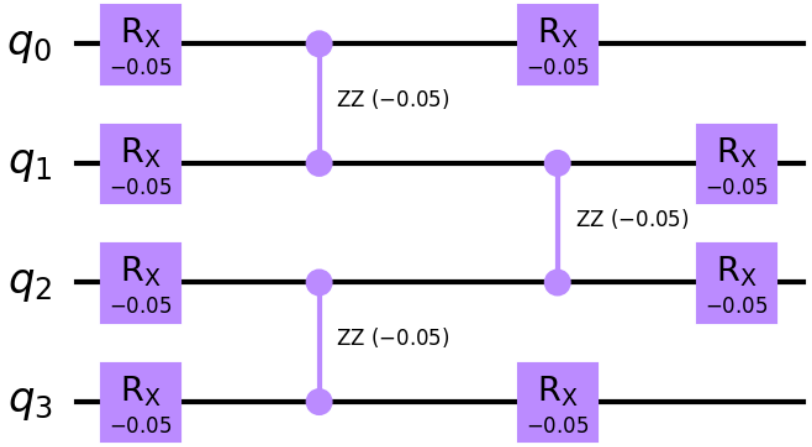

Figure 12: Second order trotterization step, which evolve the state for a time step dt.

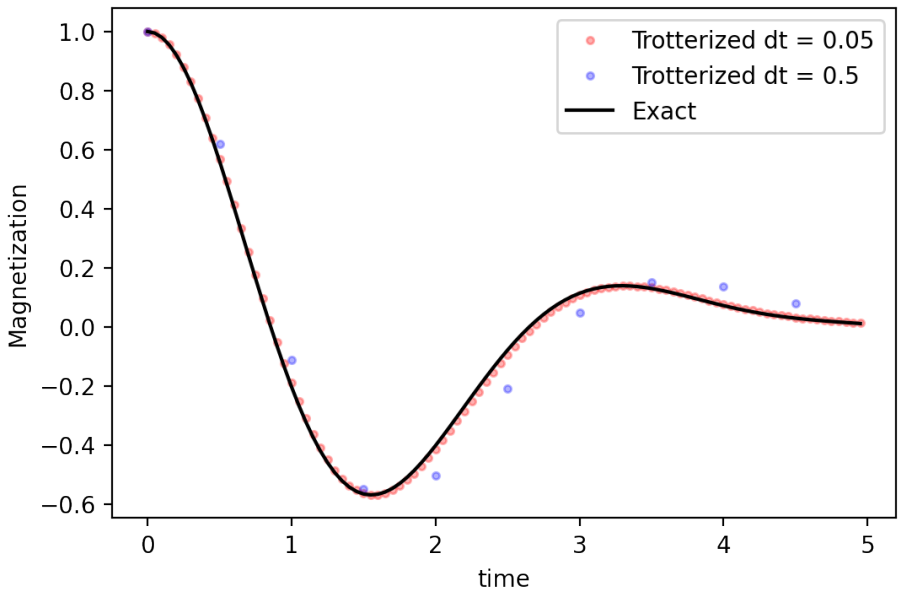

Figure 13: Time evolution of the magnetization of the TFI system, with N = 10 qubits, $|\Psi_0\rangle = |0...0\rangle$ (spin downs) and transverse field strength $g = 2$.

Exercise 7

We simulated the time evolution of the system using second order Trotterization for $N = 10$ qubits, $g = 2$, $t \in [0, 5]$ and different time steps $dt = 0.05, 0.5$. The initial state is $|\Psi_0\rangle = |00...0\rangle$ (all spins down) and we extracted the magnetization $m_z(t)$ of the system, as reported in Figure 13. Since the TFI Hamiltonian can be exactly diagonalized, it is possible to compare the trotterizated result to the exact solution. Already for $dt = 0.05$ the exact and simulated result have a similar qualitative behaviour, sufficient for the scope of our simulation: any more decrease of the time steps increases computation time without improving significantly the similarity to the exact solution.

Exercise 8

We can now evaluate the Loschmidt rates. The initial Hamiltonian is chosen as $\hat{H}(g = 0)$, so the ground state consists of 2 ferromagnetic states $|\Psi_0\rangle = |00...0\rangle$ and $|\Psi_1\rangle = |11...1\rangle$.

a) Figure 14 shows the individual rates $\lambda_{0/1}(t)$ and the Loschmidt echo $\lambda(t)$ for $t \in [0, 5]$, field strength $g = 2$, and variable number of qubits from 6 to 12. The final graph is obtained from the same parameters for 16 qubits, and it is a close-up around the intersection of the two individual rates, where the Loschmidt echo $\lambda(t)$ is expected to become non-analytic in the thermodynamic limit.

b) Here for simplicity of computation, we fixed the number of sites to 10, and varied g in the interval $[0.5, 1.5]$. As shown in Fig 15, as g is increased to around 1.0, the two individual Loschmidt rates start to intersect, and as we derived in Problem 5, the DQPT begins to emerge. For field strengths less than 1.0, we do not see a non-analytic behavior of the Loschmidt echo (which is simply the lower of the two individual rates, $\lambda_0(t)$, represented by the blue curve overlapped under the green one for $\lambda(t)$).

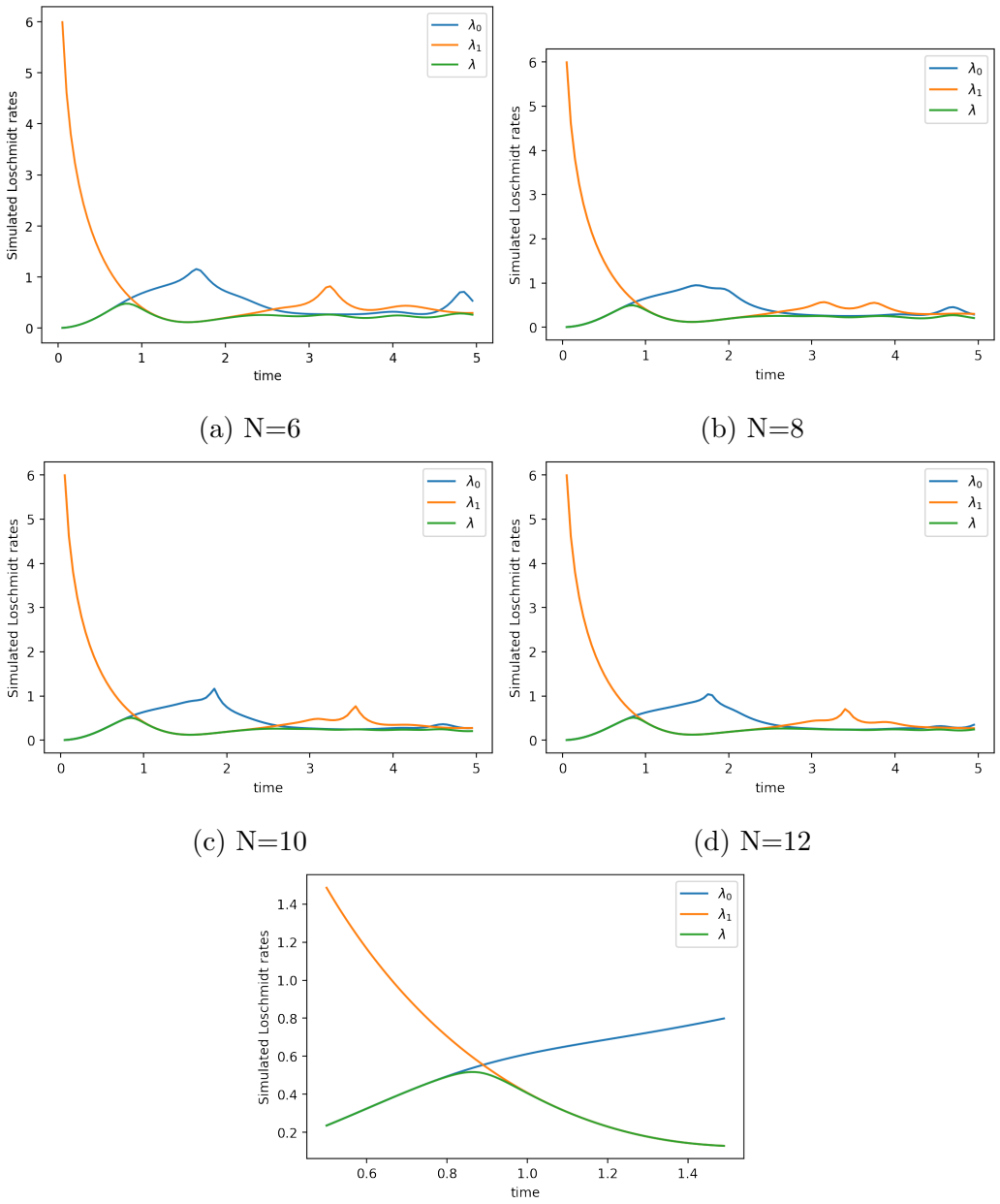

(a) N=6

(b) N=8

(c) N=10

(d) N=12

(e) N=16

Figure 14: Simulated Loschmidt rate λ and indiviual rates $\lambda_0(t), \lambda_1(t)$, for $g = 2$ and number of qubits $N = 6, 8, 10, 12, 16$.

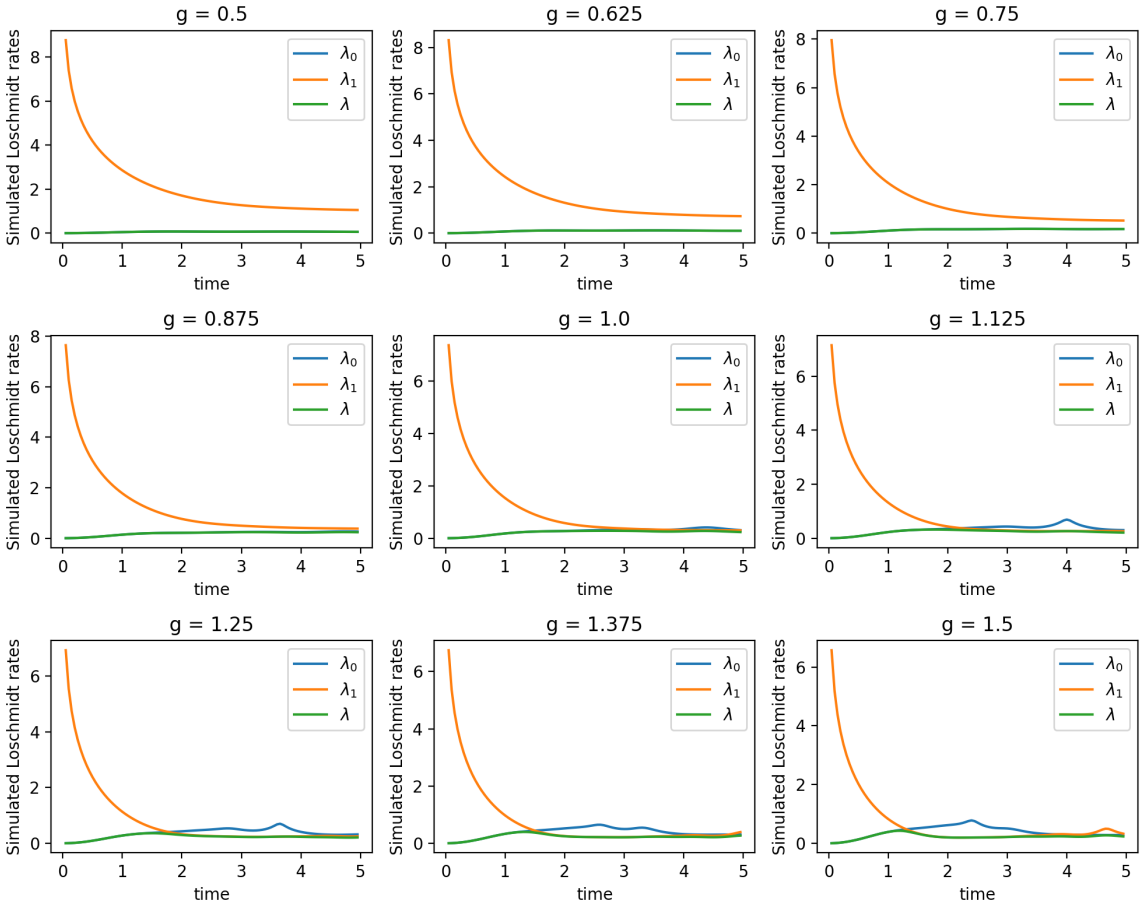

Figure 15: Simulated Loschmidt rate λ and indiviual rates $\lambda_0(t), \lambda_1(t)$, for $N = 10$ and g varying from 0.5 to 1.5.

Exercise 9

In an actual experiment, we don't have access to the actual wavefunctions, and can only determine observables via repeated measurements. The number of basis states increases exponentially as 2^N with system size, however we only need a constant/-linear number of measurements to accurately determine the magnetization and the Loschmidt rate.

For magnetization, the Hamiltonian becomes translationally invariant with increasing system size, and we can simply measure the $\langle \sigma_z \rangle$ expectation value of a single qubit thanks to this symmetry.

For the Loschmidt rate, a similar argument can be made: we're only interested in the counts in the $|00\ldots0\rangle$ and $|11\ldots1\rangle$ basis states, which can be extracted by measuring all qubits several times and extracting the number of times the results all agree.

See code implementation for the new repeated measurements method.

Exercise 10

The time evolution of the magnetization $m_z(t)$ and the Loschmidt rate $\lambda(t)$ are reported in Figure 16.

The Loschmidt rate, being an oracle for critical times t_c when the system experiences dynamical phase transitions, shows a non-analytic kink just before $t = 1$. Not-so-coincidentally, the magnetization drops to zero at the exact same time! This verifies our initial comparison of the Loschmit rate to the free energy density, except that now the non-analytic parameter dependence is on that of time, giving the Dynamic QPT its namesake.

Exercise 11

We are now interested in the production of entanglement in the system as a function of time. Specifically, we partition the system from the middle, and simulate the bipartite entanglement between these two halves. The entanglement measures we use are the Renyi entropies of order $\alpha = 1, 2$, which are functions of the reduced density

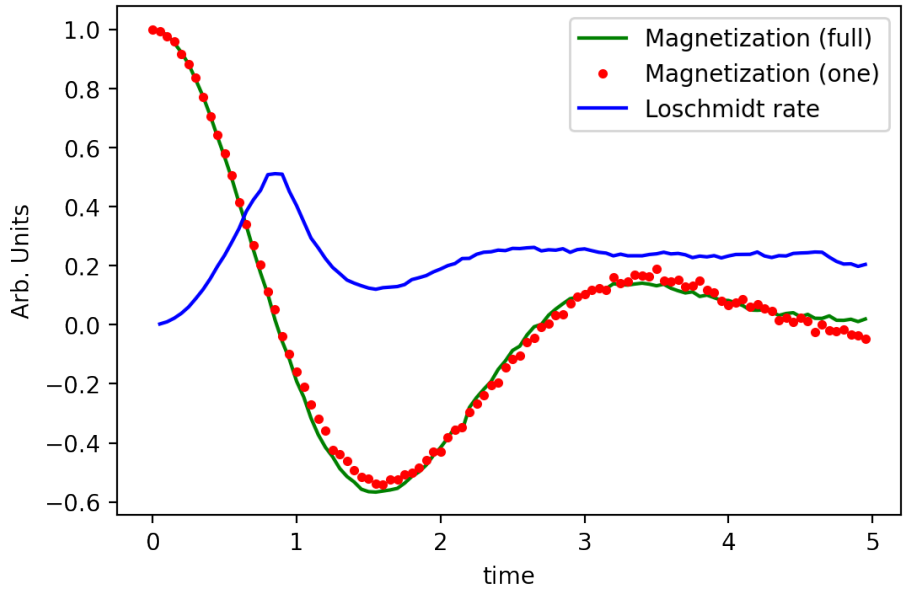

Figure 16: Simulated Loschmidt rate λ and magnetization for $N = 10$ and $g = 2$, via repeated measurements. We verify that measuring the magnetization of one qubit (red dots) accurately represents the full system (green curve).

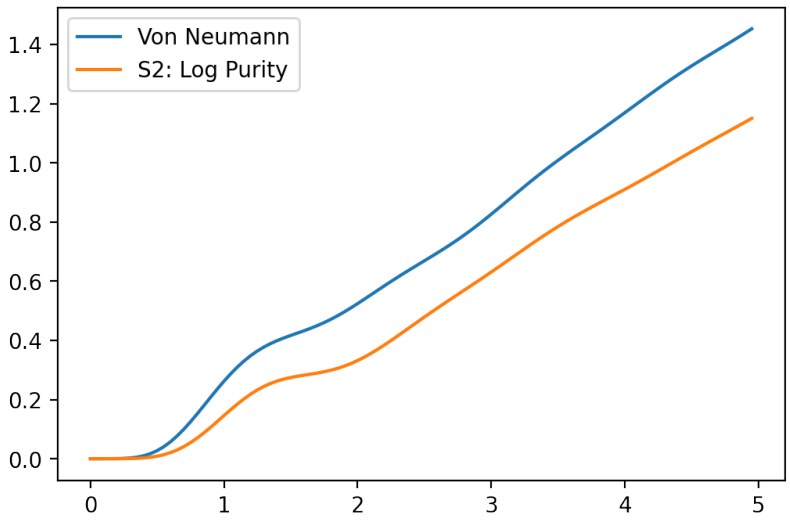

Figure 17: Entropy production during the time evolution, for $N = 10$ qubits and $g = 2$, again starting from the ground state $|\Psi_0\rangle = |0...0\rangle$

matrices $\rho_l = \mathrm{Tr}_r[\rho]$, as

$$S = -\mathrm{Tr}[\rho_l \log(\rho_l)]$$
$$S^{(2)} = -\log\big(\mathrm{Tr}[\rho_l^2]\big)$$

We calculate these quantities directly from the simulated wavefunctions. The results are shown in Figure 17. Both entropies have the same qualitative behaviour and grow linearly in time.

Exercise 13

As in Exercise 9, in a real experiment we do not have access to the wavefunctions, so we need to perform measurements on the qubits. Using the method of Randomized Measurements we get the result in Figure 18, in the same condition of $N = 10$ qubits and $g = 2$. The behaviour is not as clear as in the previous case, but we still have a somehow linearly growing function.

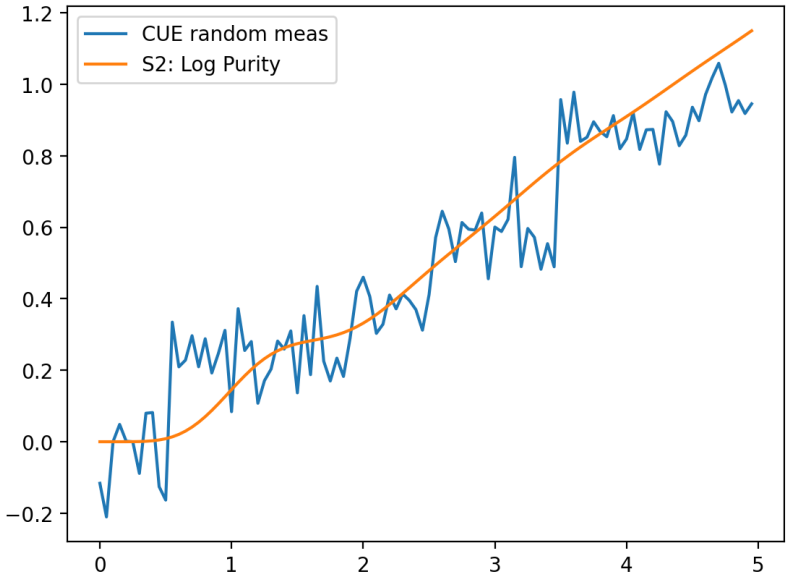

Figure 18: Entropy production during the time evolution, for $N = 10$ qubits and $g = 2$, with randomized measurements on the qubit.